11

Industrial Sprays: Experimental Characterization and Numerical Modeling

Avinash Khopkar[1], Michael D. Cloeter[2] and Quan Yuan[2]
[1]*Dow Chemical International Pvt. Ltd., Pune*
[2]*The Dow Chemical Company, Freeport, TX*
[1]*India*
[2]*USA*

1. Introduction

Sprays in industrial processes are becoming more common as well as more challenging for design. Spray formation processes are critical to the performance of a number of technologies and applications. The spray applications can be quite varied and include combustion systems (gas turbine engines, internal combustion engines, incinerators, furnaces, rocket engines), agriculture (pesticide and herbicide treatments), paints and coatings (furniture, automobiles), consumer products (cleaners, personal care products), fire suppression systems, spray cooling (materials processing, computer chip cooling), gas treatment (thermal quench, acid neutralization), medicinal/pharmaceutical, reactor feed injections, liquid distribution into chemical units (defoaming, uniform flux over column packing), and spray drying (foods, drugs, materials processing).

The process requirement varies depending upon the application. For example, making small drops are important for internal combustion engines and other applications where rapid mass transfer into the gas phase is critical. Large drops may be desired where entrainment in a counter-current gas flow must be minimized. In another case, creating a narrow drop size distribution, neither too small or too large, is desired for agricultural sprays when trying to achieve low driftable fines while at the same time maintaining good target coverage.

Controlling the spread of drop distribution plays very important role in paints and coatings, consumer products, medicinal delivery, and spray drying applications. On the other hand, distributing liquid mass more uniformly throughout the spray and increasing the fraction of liquid that impacts a target are key requirements in paints and coatings, spray cooling, and fire suppression applications.

Injector designers face challenges in designing the atomization process for achieving the desired process output. Despite immense progress in laser diagnostics for spray flows, the reliable experimental data on atomization characteristics are still scarce due to measurement difficulties associated with the dense spray zones formed around the liquid jet core. As a result, application of empirical correlations for atomization flow characteristics has a very narrow range of applicability. It is therefore, essential to develop and apply new tools to enhance our understanding of the atomization process. Such an understanding will be useful in devising cost effective and reliable scale-up of spraying operations.

Research support for industrial processes and products must advance with these challenges. This involves both experimental and numerical capabilities. It is important to critically evaluate the current understanding of experimental and numerical capabilities and translate this understanding into improving spraying operation. Such an attempt is made here.

2. Experimental methods for spray analysis

Imaging methods such as laser-induced fluorescence are used to track velocity profiles before, during, and after liquid film breakup, as well as to track distribution of mass flux and drop size distribution (DSD). Governing liquid break-up regimes depend on level of turbulence and interactions with gas phase, and can include unstable jets, waves, perforations, and secondary atomization. The interaction of micro-structured liquids with turbulence can have a profound impact on breakup dynamics. Even slight formulation changes can have unexpectedly large impact on the spray properties.

Multiple examples have been chosen for illustrating the variation in spray problems encountered in practice. Certain commonalities in the analysis are evident regardless of the spray problem.

In industrial problems, not all sprays can be studied in a lab setting using state-of-the-art laser diagnostics. Frequently, the spray may consist of a relatively large flowrate (100+ gpm) that is not amenable to laboratory research. The researcher needs facilities to characterize such large sprays, including gas-assisted sprays. The authors' facilities have a nozzle test stand for evaluating such sprays. See Figure 1.

Fig. 1. Interior and exterior view of the nozzle test stand at The Dow Chemical Company, Freeport, Texas, USA.

The use of an enclosed structure is necessary due to the dangerously loud noise levels generated by certain sprays, particularly industrial gas-assisted sprays. A blower and stack is included to assist air flow and prevent mist accumulation inside the test stand building. Rented pumps and compressors are brought to the stand when the needs of the project exceed the capability of permanent pumps and the plant air utility.

At other times, the researcher must go to the spray, which can be in a plant or pilot facility. Thus the tools of researcher must include an array of capabilities. The tools described herein vary from the very simple and portable to the more complex and fixed methods that have been used by the authors. The following descriptions start with the simplest options and continue to describe those that are more complex.

2.1 Flash photography

Flash photography is a basic method that allows one to capture a view of a spray over the small duration (< 0.1 ms) of the flash. This is often a short enough exposure that the spray appears frozen in time. Important basic features of the spray can be revealed such as spray angle, symmetry of the bulk flow, distance of the breakup zone, breakup mechanism, and basic shape of the mass distribution (when viewed from several angles). The effect of flow rate on each of these variables can also be studied.

This method, along with video, has been extremely useful to the authors for initial characterization of many sprays. It can be used in "out-of-lab" environments such as the test stand shown in Figure 1 and production plants. Figure 2, for instance shows comparisons from the test stand and a plant thermal quench arrangement. The flow rate exceeds 100 gpm.

Fig. 2. Left, image of an axially-vaned thermal quench nozzle in operation in the authors' test stand**.** The aim of this test was to quantify the spray angle and asymmetries of the plant nozzle**.** Several flow rates and nozzle designs were tested**.** Right, field test in plant.

This method has been used for viscous and non-Newtonian sprays as well. Figure 3 shows images from a tangential whirl nozzle with flow of a 200 cP corn syrup-water solution. While this solution can be considered Newtonian, the effect of shear-thinning or other non-

Newtonian behavior on nozzle performance can also be quantified by testing solutions with a low-shear viscosity near 200 cP.
The Reynolds number for the conditions of Figure 3 is 500. It can be seen that the observed spray angle of 60 degrees is substantially less than the published (water) spray angle of 90 degrees. It is also seen that an "S"-shaped pattern is observed as opposed to the hollow cone observed for water. The sheet breakup starts at 6 inches from the nozzle tip. Perforated sheet breakup is observed, as well as Rayleigh-Plateau instabilities near the edge of the spray.
All of these characteristics are observed through a standard digital SLR camera. Many nozzles can be tested in this way in a single afternoon in order to find the right nozzle for a given application.

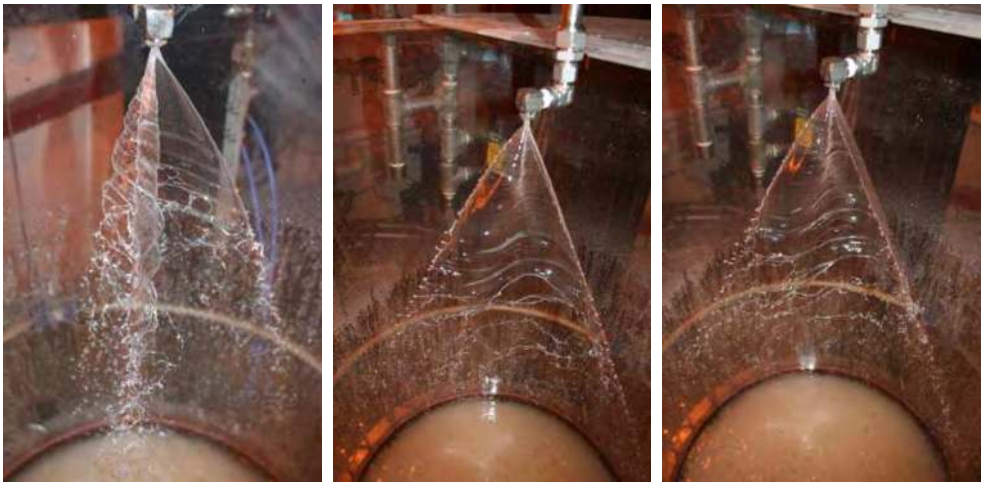

Fig. 3. Tangential whirl nozzle with 200 cP corn syrup/water solution**.** Flow conditions 27 psi, 1.45 gpm, Reynolds number based on the orifice diameter is 500.

2.2 High-speed imaging

High-speed imaging is a method that can give an estimate of the velocity of the spray by comparing images that are a known time increment apart. For dense sprays, the analysis may be limited to the exterior portions. The individual droplets may not be accessible, but we have found that movement of *structures*, consisting of groups of drops, is sufficient to get a reasonable estimate. High-speed imaging has also been extremely useful for discovery of non-idealities such as pulsations in the flow. These can arise, for instance, from cavitation inside the nozzle or from sub-optimal interior contacting in gas-assisted flows.
An example occurred in a spray nozzle used for a liquid injection of an additive into a gas-phase reactor. By the naked eye, the spray (as reproduced in the lab) looked perfectly acceptable. High-speed imaging, however, showed pulsations (or "surges") in the spray flow that were beyond the ability of the naked eye to perceive. Example images from 1000 Hz imaging are shown in Figure 4. The images of the figure are sequential, showing that the duration of pulses was less than 2 ms. Examination of several seconds of data showed that the pulses occur at a frequency of 50 Hz, above the naked eye perception of ca. 20 Hz. More will be covered on the problem in the *PLIF Imaging* section.

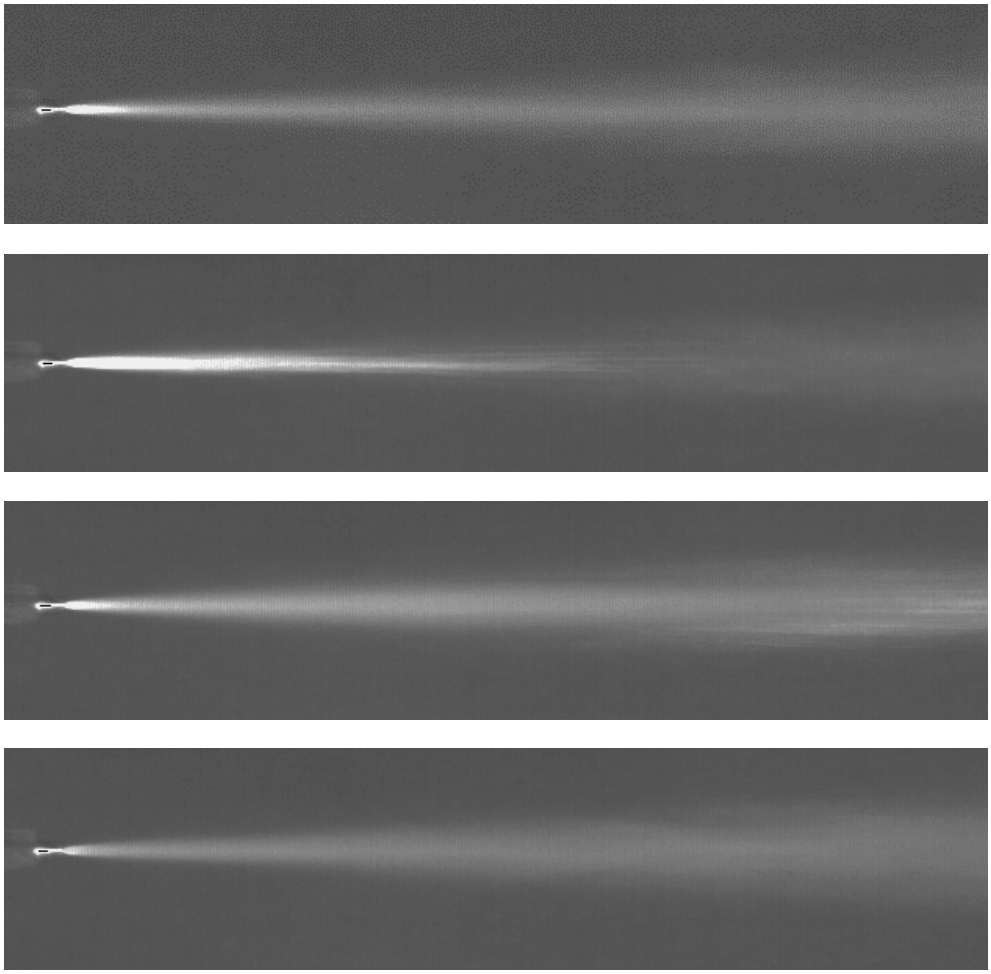

Fig. 4. Consecutive high speed images showing the pulsation effect from an injection nozzle. A frequency of 1000 Hz was used in the imaging. The pulsation frequency was measured as 50 Hz.

Although high-speed cameras are sensitive equipment, they have sufficient portability that we have used them in outside-the-lab environments at reasonable ambient conditions. Figure 5, for instance, shows consecutive images of a dense air-assisted spray that was running in the nozzle test stand. The velocity profile was needed for boundary conditions of a CFD model. Velocities of 60 – 100 ft/s were measured, with the magnitude dependent on the location. In dense sprays, reasonable estimates for velocity can be provided by watching the motion of flow features in the spray, then applying velocimetric principles [Raffel *et al*., 1998]. Near the edge, tracking the motion of groups of individual drops is also useful.

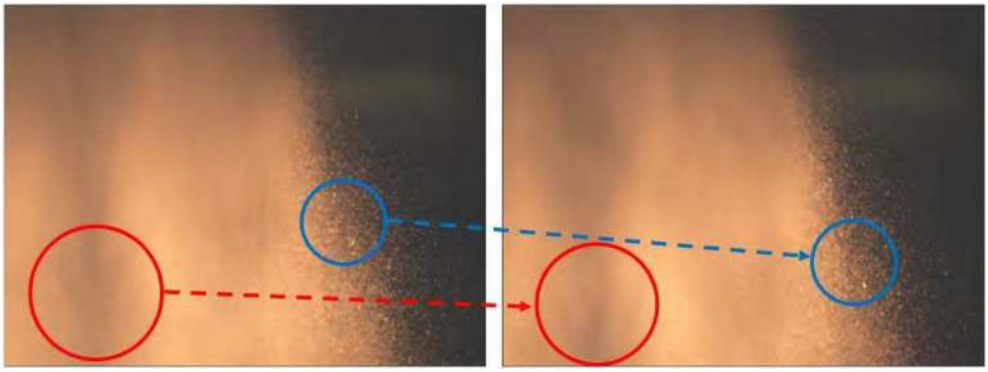

Fig. 5. High speed images (1000 Hz) showing how flow features and collections of drops are used to estimate velocity locally using velocimetry principles**.** This example is from a dense air-assisted spray located outside the authors' laboratory, hence outside the realm of our laser diagnostics**.**

2.3 PLIF imaging

When a small amount of a fluorescent dye is added to the feed liquid, Planar Laser-Induced Fluorescence (PLIF) can be used to capture detailed images of the spray as it issues from the nozzle. A plane of pulsed laser light (duration 10 ns) is aligned to pass through the axis of the spray. A camera is aligned perpendicular to the laser plane. The system is synchronized so that the laser pulsates while the camera shutter is open. Figure 6 shows a photographic

Fig. 6. Photograph taken during a PLIF imaging experiment utilizing a Dantec Dynamics FlowMap System Hub.

image taken during a PLIF experiment to best illustrate the method. In velocimetry mode, dual images using dual laser pulses are taken on the order of 10 to 100 μs apart. The movement of the spray structure or droplets themselves over the known time increment is used to calculate the local velocity. The method has been shown to give consistent velocity results before, during, and after the droplet formation. The velocity distribution can give some information on expected mass flux pattern. However, the method doesn't distinguish between large and small droplets or account for the variable spatial concentration of droplets, so strictly speaking an actual flux cannot be computed from the velocity vector results. Averaging of many PLIF images can give useful information on mass flux within the slice of the spray that is illuminated.

Figure 7 shows a PLIF image of an agricultural spray and the corresponding averaged velocimetric data taken from 500 image pairs. The vectors form a fairly continuous contour that is consistent with the characteristic shouldering of the spray flux.

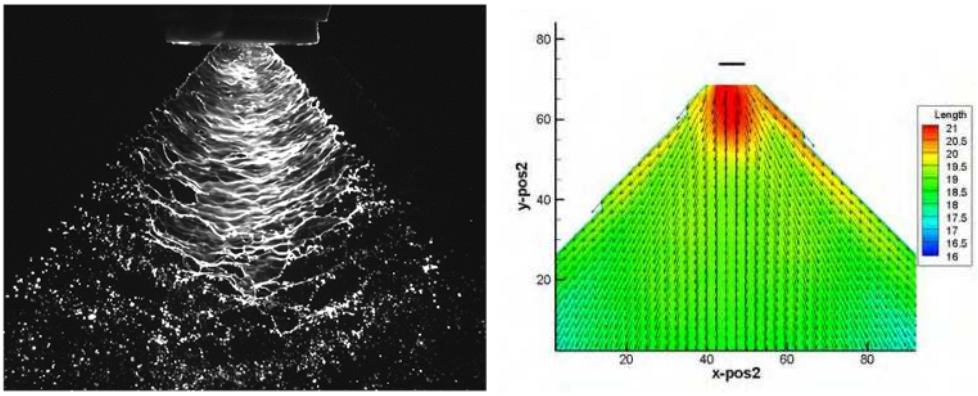

Fig. 7. Left, example PLIF image of a flat fan agricultural spray, Spraying Systems Co. TeeJet 8002**.** Right, velocity contour plot with overlaid vectors, average of 500 image pairs**.**

Figure 8 shows PLIF imaging of the same spray as is shown in the high-speed images of Figure 4. The short 10 ns duration of the laser is sufficient to provide rich detail on the spray structure. The pulsating nature of the spray is again evident by comparing images. The PLIF image allows quantitative calculations to estimate the amount of mass issued in the pulses (or "surges") compared to the baseline flow between pulses.

Figure 9 shows a comparison of Mie Scattering and PLIF imaging. The Mie Scattering is sensitive to surface area whereas PLIF imaging is proportional to volume. It is easily noted that a large fraction of the spray volume is present on the outside edges of the spray, and at the same time there are many small droplets present in the interior portion.

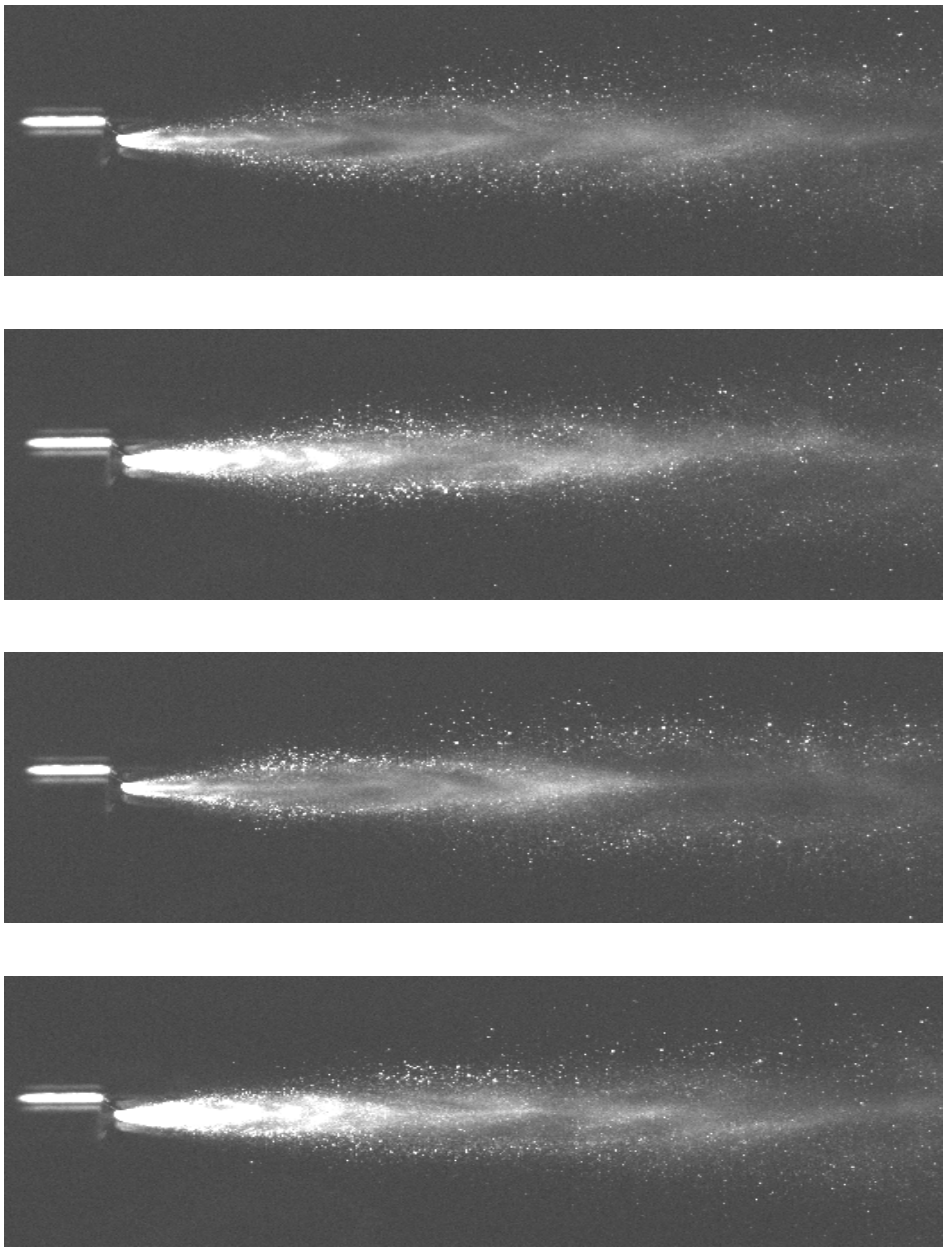

Fig. 8. For the identical nozzle as shown in Figure 4, PLIF imaging at 5 Hz was used to better understand the flow characteristics during and between pulsations.

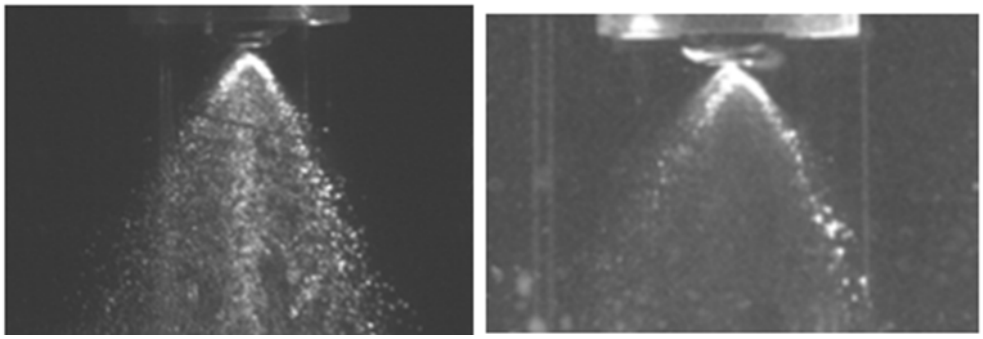

Fig. 9. Mie Scattering (left) and PLIF (right) images, showing surface area versus volume effect.

2.4 PLIF patternation

Similar to the PLIF velocimetry approach, the laser is turned 90 degrees to be orthogonal to the axial direction of the spray. Approximately 10,000 images are taken and averaged, as is shown in Figure 10. Depending on the density of the spray, it may not be possible to permeate the entire spray cross-section, making it necessary to assume symmetry.

Optical patternation techniques are particularly useful when the fluid to be sprayed is hazardous. This can occur, for instance, when spraying active herbicide formulations. The authors' lab uses a transparent ventilated spray enclosure, constructed of acrylic and glass, to protect personnel from contact with the hazardous fluid. The sprayed liquid is fully collected and optionally recycled in order that the amount of waste generated in an experimental series is reduced. The enclosure is also useful for high mist-generating sprays to prevent mist accumulation onto sensitive electronic equipment.

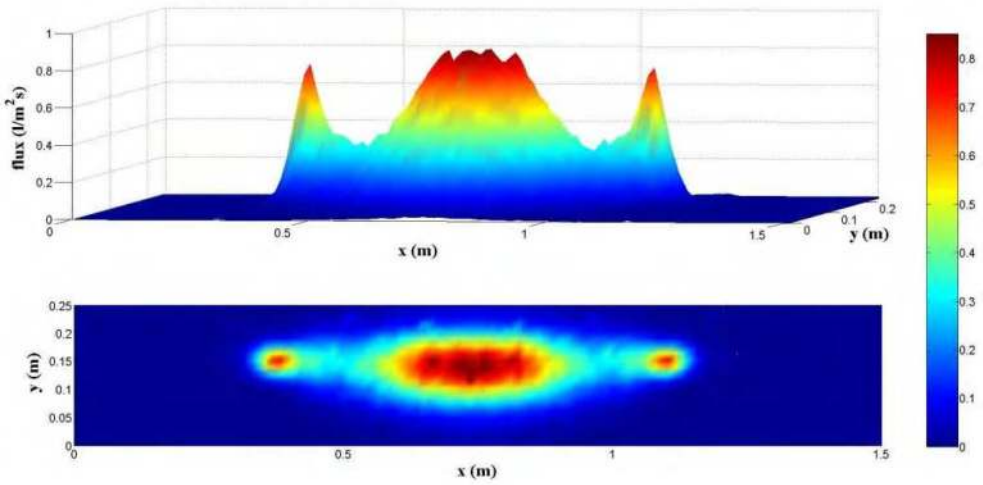

Fig. 10. Patternation results from the averaging of 10K PLIF images.

2.5 Mie scattering for scalar mixing

In cases where the measurement of gas motion and scalar mixing are important to characterize the spray, a fog has been employed to mark the gas flow. In one such method, air is fed to the system which has first been passed sequentially through aqueous solutions of hydrochloric acid (HCl) and ammonium hydroxide (NH_3OH), which efficiently generates a fog of ammonia droplets. This was employed in the apparatus shown in Figure 11. In this case, the fog was introduced in a shroud around the spray nozzle. Commercial oil-atomizing or glycerin-atomizing devices are also available to generate fogs. Smoke-generating testing devices, used to test for negative pressure, can also be employed to qualitatively view the air flow induced by a spray.

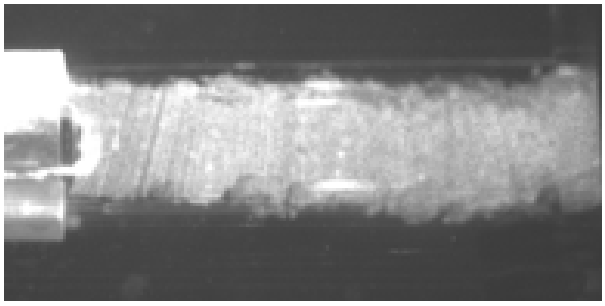

Fig. 11. Mie scattering of a shroud fog introduced around a spray nozzle to examine scalar mixing**.** The spray nozzle was off when this image was taken.

2.6 Mechanical patternation

The authors have utilized both one-dimensional and two-dimensional mechanical patternation techniques. For sprays with relatively small flowrates (< 0.5 gpm), an arrangement of ½" x ½" cuvettes has been utilized to look at two-dimensional patterns. A hinged door covers the cuvettes until the desired flow conditions through the spray nozzle have been established, then the door is rapidly opened. As the fastest-filling cuvette(s) approach full level, the door in returned to its original position and flow is stopped. The contents of each cuvette is then carefully weighed. Figure 12 shows the method and results.
Sometimes, 2-D patternation is desired to look at subtleties in the flow pattern at the outside edges and to look at, for instance, turbulence history indicators in the sprayed solution. One such example is spraying of emulsions to study drop size distribution of an oil phase before and after spraying as a function of position in the patternator.

2.7 Dynamic image analysis

We have used this method to capture images of the spray droplets which are then processed in real time. A strobe is used to backlight the imaged area, which is typically of dimensions near 1 cm x 1 cm. Out-of-focus drops are removed from the analysis by defining a sharpness criterion for the droplet. Partial drops, extending beyond the edge of the images, are also removed. Non-spherical droplets are converted to an equivalent diameter by matching the projected area. A sufficient number of images are taken at 30 Hz to achieve converged drop size distribution, commonly 50,000 to 100,000 validated drops. The frequency can be adjusted based on expected drop velocity to assure that the same drops are not counted more than once. Figure 13 shows a sample image taken from dynamic image analysis of a flat fan agricultural spray.

This type of size analysis is commonly used in the authors' lab for nozzles with relatively small-scale flows, although the nozzle test stand of Figure 1 also uses this type of drop size analysis.

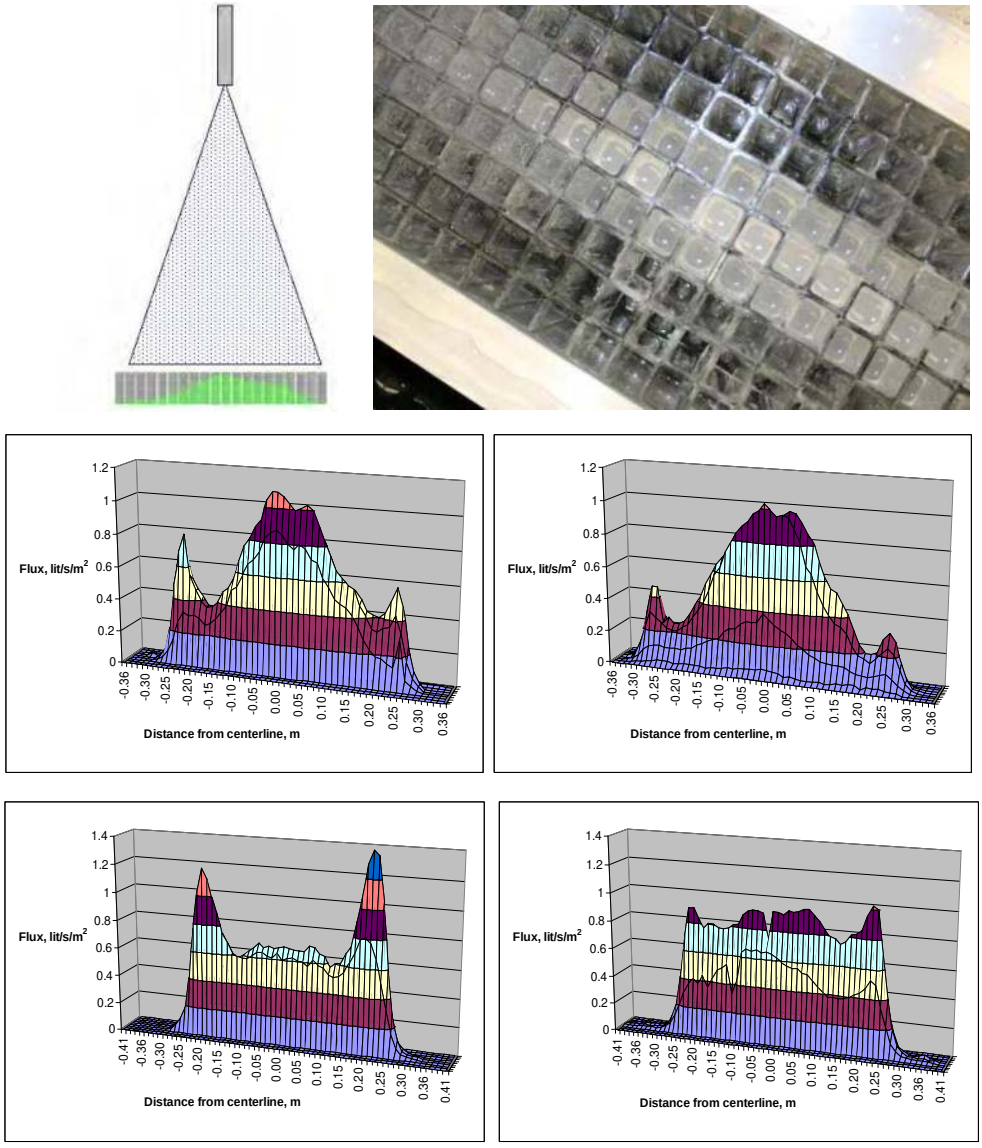

Fig. 12. Mechanical patternation. Upper left, general concept. Upper right, filled cells from a 2-D patternation measurement of a flat fan spray. Middle images, 2-D patternation results from a Spraying Systems Co. Teejet 8002 nozzle under identical conditions except for a formulation change to the sprayed liquid. Bottom images, Teejet 8002E nozzle at same conditions as the Teejet 8002 in the middle images.

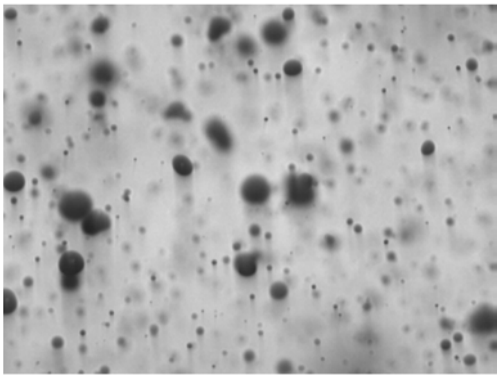

Fig. 13. Sample dynamic image from an agricultural spray.

2.8 Summary of experimental methods

The analytical needs of the researcher varies from spray to spray and project to project. In some cases, only verification of spray angle is needed for a custom industrial installation or for a series of similar but slightly different nozzles. At the other end of the extreme, there are situations where information on velocity profile, drop size, and mass flux distribution are needed to parameterize the inputs to a CFD model. In other cases, the impact of changes in formulation need to be elucidated based on changes to film breakup dynamics and drop size. The experimental tools described here have been able to provide the required information for a wide variety of industrial problems encountered.

3. Computational methods for spray analysis

In last two decades, several attempts have been made using Eulerian-Lagrangian (E-L) computational fluid dynamics (CFD) based models for simulating spraying. However, well established E-L CFD models for fluid flow and evaporative/reactive spray dynamics are sensitive to spray origin parameters, such as initial droplet size distribution, initial velocity and droplet number density. These spray origin parameters are controlled by primary atomization. Advanced mathematical models for primary atomization are needed to compute time-averaged and transient characteristics of droplet formation. Recent advances have been made using computational model for developing better understanding on the primary atomization process (Gorokhovski and Herrmann, 2008; Bini et al., 2009; Herrmann et al. 2011). However, these studies demand significant computational time and resources even for idealized flow conditions (e.g. nonreactive system).

3.1 Primary atomization

3.1.1 Eulerian-Eulerian approach for modeling primary atomization

In the Eulerian-Lagrangian approach for modelling spray behavior, the atomization process is typically modelled using a surface wave instability model that predicts spray parameters such as the spray angle and droplets' diameters. The surface wave growth models widely used include the surface wave instability model [Reitz and Diwakar], the Kelvin-Helmholtz/Rayleigh-Taylor (KHRT) instability model [Patterson and Reitz] and the Taylor Analogy Breakup (TAB) model [O'Rourke and Amsden]. The effect of nozzle geometry on the primary atomization is approximated using an empirical nozzle-dependent constant,

which require experimental data or experience to give reliable predictions. With the high performance computing (HPC) system becoming more powerful and less costly in recently years, it is becoming more feasible to directly model the primary atomization by resolving the gas-liquid interface evolution and breakup use an Eulerian-Eulerian approach [Gorokhovski and Herrmann].

Immiscible fluids interface tracking can be done using several approaches in the Eulerian framework: the front tracking method [Unverdi and Tryggvason, 1992], the volume of fluid (VOF) method [Hirt and Nichols, 1981] and the level set method [Osher and Sethian 1988, Sussman 1994]. The front tracking method, which tracks the motion of the surface marker particles attached to the gas-liquid interface, has numerical limitations for three-dimensional irregular interfaces. It is therefore not popularly used for predicting primary atomization. In the VOF method, the volume fraction of a fluid (i.e. the liquid phase) α is solved for each of the computational cells:

$$\frac{\partial \alpha}{\partial t} + \mathbf{V} \cdot \boldsymbol{\nabla} \alpha = 0 \tag{1}$$

$$\alpha = \frac{1}{V_{cell}} \int_{V_{cell}} H(x, y, z, t) dx dy dz \tag{2}$$

The nature of the VOF model ensures mass conservation. Because the method takes a volumetric approach to track the interface motion, numerical diffusion is inevitably inherent in the model. Special numerical algorithms are available for reconstructing the interface shape and minimizing the numerical diffusion [Youngs 1982, Ubbink 1997, Muzaferija et. al. 1998]. Surface tension is typically implemented as a volumetric force using the continuum surface force (CSF) method [Brackbill et. al. 1992].

Figure 14 shows the predicted jet breakup to form droplets for a laminar jet using the VOF method, showing good agreement with the measured droplet sizes.

In the level set method, a scalar equation representing the signed distance from the interface is solved:

$$\frac{\partial \phi}{\partial t} + \mathbf{V} \cdot \boldsymbol{\nabla} \phi = 0 \tag{3}$$

The interface is described with the zero level curve of the scalar. For ensuring the scalar function to remain the signed distance to the gas-liquid interface, a redistancing algorithm is typically applied. This can generate mass loss in under-resolved regions. This can be reduce by refining the computational mesh for avoiding under-resolved regions or taking the coupled level set VOF (CLS) approach [Mikhael Gorokhovski and Herrmann, 2008]. Figure 15 gives a snapshot of the predicted drops using the coupled level set VOF method [Liu,Garrick and Cloeter, 2011].

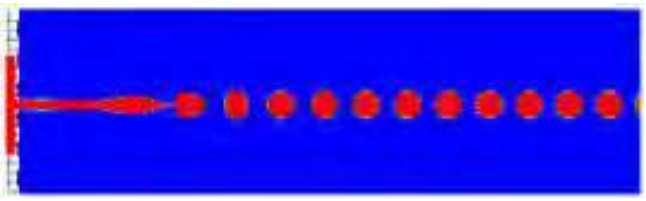

Fig. 14. Predicted droplets formed due to the Rayleigh-Taylor instability using the VOF method, showing good agreement with measured droplet sizes.

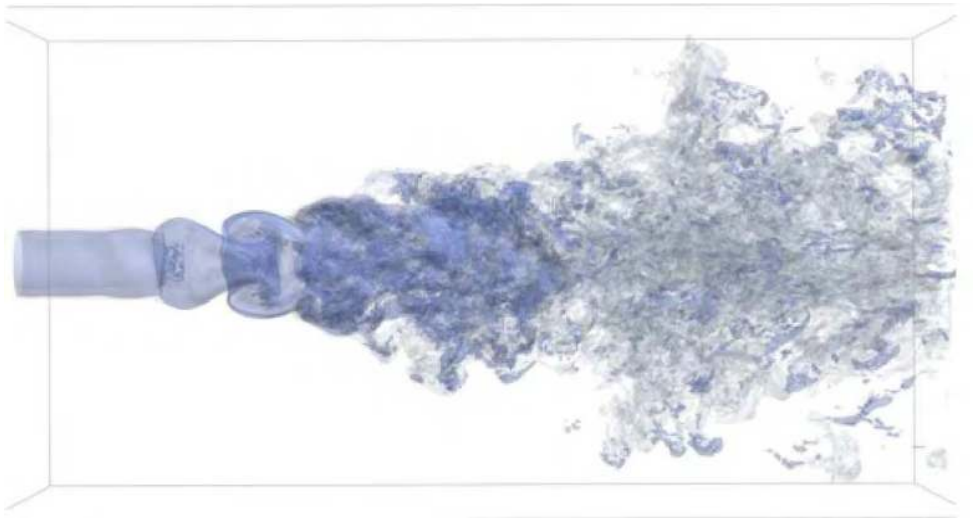

Fig. 15. Predicted primary atomization using the coupled Level Set - VOF method [Liu, Garrick and Cloeter, 2011].

3.2 Coupling reaction, flow and spray dynamics

Computational implementation of coupled primary atomization, two-phase spray model, simultaneous heat and mass transfer and subsequent reaction is a challenging and difficult task. The major difficulty in primary atomization simulation is disparity between the time and length scales in liquid core and gas phase domain. Efficient computational approaches need to be developed to resolve the numerical stiffness due to the coupling between the jet transport equation and gas phase dynamics near nozzle. Furthermore, adequate topological representation of the three dimensional jet core shape and the surrounding gas computational grid needs to be established. The volume of fluid (VOF) method is used to capture gas-liquid interface (Liang and Ungewitter). However, VOF requires very high grid resolution for resolving jet surface. Therefore, including primary atomization in simulating reacting sprays become a huge challenge with respect to computational demand. In the majority of CFD simulation of spray combustion, the atomization process is presented in terms of a point or surface source of droplets with a prescribed size distribution introduced at the nozzle exit. The subsequent breakup and coalescence of the droplets are modelled based on the droplet Weber number criteria. This approach uses the assumption that the dynamics and breakup of liquid jet indistinguishable from those of a train of drops. In this work, a CFD model is presented using the above described approach to simulate reacting spray dynamics.

The particle formation in the fluid bed reactor is a complicated process involving multiphysics. It is affected by many factors such as the dispersion of catalyst drops, the solvent evaporation rate (if it is used for dissolving solid catalyst), the mass transfer of reactant gas into the catalyst drops and the reaction kinetics. The nozzle operating conditions and design of the injection nozzle control the dispersion of catalyst droplets in the dilute zone. Whereas, the mass transfer to and from the droplets and the interaction between the droplets are controlled by the quality of droplet dispersion in the dilute zone. This indicates complex interactions between the operating conditions (shroud velocity),

reactor hardware (nozzle design) and performance (dispersion of droplets and rates of transport processes). Due to the complex physics involved, it is advisable to break the complex process into multiple simpler sub-processes for better understanding of their effects on the overall process. The above discussed problem is broke into two parts. In the first part, CFD model was developed to understand the influence of the operating conditions and prevailing fluid dynamics on the dispersion of catalyst droplets. Whereas, in the second part CFD model was developed to understand the influence of prevailing fluid dynamics on the mass transfer and on the growth of polymer particles. The methodology is summarized in Figure 16. The findings from both the parts generate more understandings on how to control the final particle size distribution in the reactor.

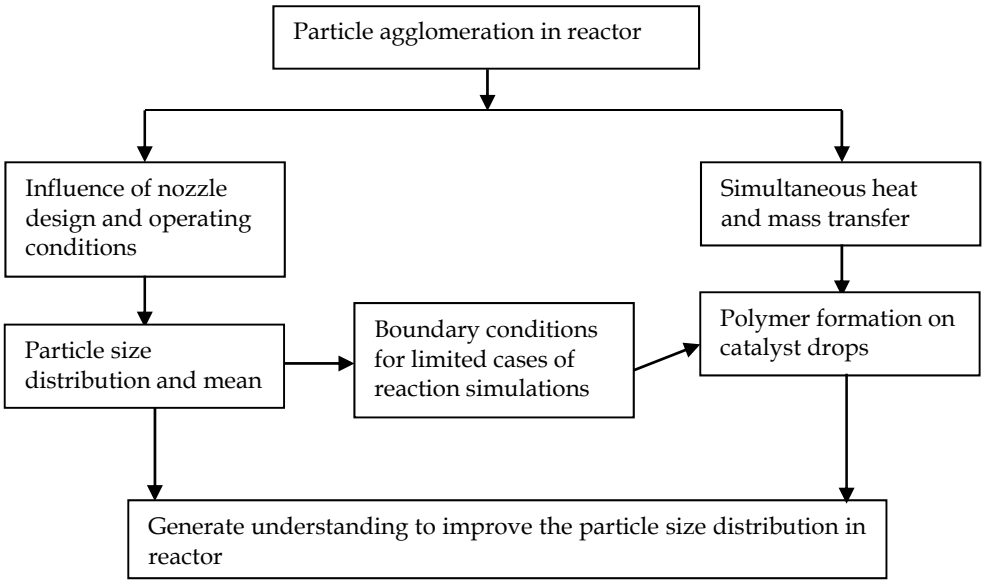

Fig. 16. Problem Solving Methodology

3.2.1 CFD model and boundary conditions

Flow simulations were conducted using the commercial CFD package FLUENT 6.4. A few approximations were made while formulating the CFD model. Flow of different gas phase components was modeled using species transport equations. The mass flow rates of each feed stream are listed in Table 1. Ideal gas densities of each gas streams were calculated before the simulation for the given reactor pressure and temperature and were then specified in the CFD model. This approach allows us to use the incompressible flow formulation. Accurate prediction of turbulent quantities is important for reasonable prediction of the spreading rate of the jet. In the present work, the realizable k-ε turbulence model was used to simulate the turbulent flow for its better prediction of turbulent jets.

Simulations were carried out in a section of the fluidized bed with the height equal to the diameter (H/D= 1). The schematic of the computational domain is shown in Figure 17. The

bottom cross section of the domain was modelled as a velocity inlet with a uniform distribution of all gas phase components. The top surface of the computational domain was modelled as a zero gradient boundary condition. The gradients normal to the outlet boundary were set to zero for all the variables except pressure.

Feed stream	Velocity, m/s
Bottom feed	0.5
Support tube	16 32
Catalyst injection	150
Catalyst drop	150

Table 1. Mass Flow Rates for Different Inlet Streams

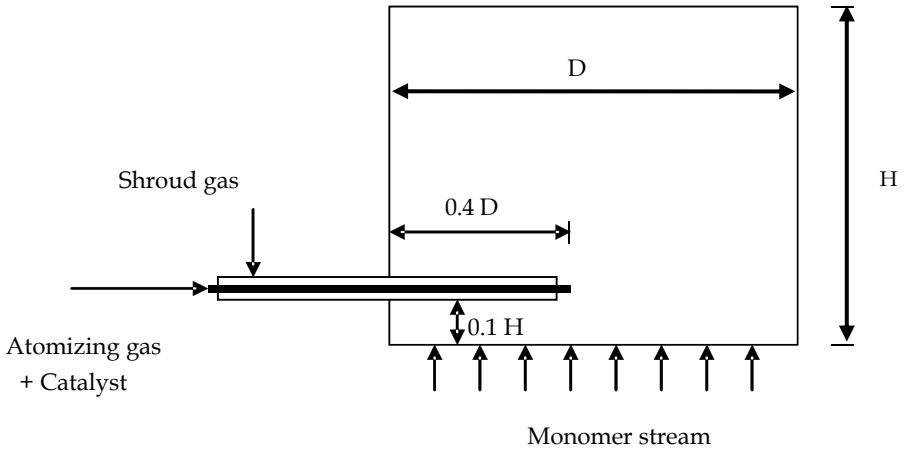

Fig. 17. Schematic of the Computational Domain

The dispersion of catalyst droplets in the domain was simulated using the Lagrangian approach. In addition to solving transport equations for the continuous phase, FLUENT allows you to simulate a discrete second phase in a Lagrangian frame of reference. This second phase consists of spherical particles (which may be taken to represent droplets or bubbles) dispersed in the continuous phase. This modelling approach is commonly called as discrete phase modelling (DPM). DPM computes the trajectories of these discrete phase entities, as well as heat and mass transfer to/from them. Trajectories of the secondary phase were calculated using discrete phase inertia, hydrodynamic drag, gravity force and other interphase forces.

$$\frac{du_p}{dt} = F_D\left(u - u_p\right) + \frac{g_x\left(\rho_p - \rho\right)}{\rho_p} + F_x \tag{4}$$

Where F_x is the additional acceleration (force/unit particle mass) and $F_D(u\text{-}u_p)$ is the drag force per unit particle mass.

The dispersed phase particles are not passive contaminants and the presence of these particles may influence the flow of the continuous phase. The level of interaction becomes especially complex for a turbulent flow field. Secondary phase loading and the number density of particles determine the level of interaction or degree of coupling between the continuous phase and dispersed phase. Depending on the degree coupling (one way, two way or four way), solutions of the both phases interact with each other (see Ranade, 2002 for more details). Due to the strong interaction of between the droplets and the surrounding fluid, in the present work, four way coupling: continuous phase-dispersed phase particles-dispersed phase particles-continuous phase, was used.

When the continuous phase flow field is turbulent, its influence on particle trajectories needs to be represented in the model. The situation becomes quite complex in the case of two-way and four-way coupling between continuous phase and dispersed phase, since the presence of dispersed phase can affect turbulence in the continuous phase and vice versa. For such cases, it is necessary to calculate the trajectories of a sufficiently large number of particles using the instantaneous local velocity to represent the random effects of turbulence on particle dispersion. The instantaneous velocity is equal to the mean velocity (which is known) plus a fluctuation velocity (which is unknown). Predictions using a turbulence model may give values of variance of the fluctuating velocity. The assumption of a Gaussian distribution for the fluctuations and a random value for fluctuation to be added to the mean velocity is not sufficient to obtain the instantaneous value. Instantaneous values should satisfy the Lagrangian correlation coefficient along the trajectory. Several models have been proposed to estimate the instantaneous velocity. See, for example, reviews by Sommerfeld (1993) and Gouesbet and Berlemont (1999). Two commonly used models to estimate instantaneous fluid velocity from the time-averaged flow field of the continuous phase are discrete random walk (DRW) model (Sommerfeld, 1990) and continuous random walk (CRW) model (Thomson, 1987). In the present study the DRW model was used. In this model, the fluctuating component of the velocity is assumed to have a Gaussian distribution and is calculated by multiplication of a normally distributed random number and the local root mean square (rms) value of the velocity fluctuations. The same value of random number is used for the eddy lifetime (integral time scale). For each eddy lifetime, new value of random number is used. This stochastic process generates a correlation coefficient which linearly decreases from 1 at a delay equal to zero, to 0 at a delay equal to twice the eddy lifetime. Despite such a crude approximation for the correlation coefficient, this approach leads to reasonable results (Sommerfeld, 1990).

It is necessary to model the droplet collisions, breakup and coalescence to simulate the spray realistically. In the present work, the droplet collision model, available with FLUENT™, was used to simulate the droplet collisions. The O'Rourke collision algorithm was used for computationally efficient spray calculation. The O'Rourke method is a stochastic estimate of collisions. It makes the assumption that two parcels may collide only if they are located in the same continuous-phase cell (O'Rourke, 1981). This assumption is valid only when the continuous-phase cell size is small compared to the size of the spray. Once it is decided that

two parcels of droplets collide, the algorithm further determines the type of collision. Only coalescence and bouncing outcomes are considered. The probability of each outcome is calculated from the collisional Weber number. This collision model assumes that the frequency of collisions is much less than the particle time step. Also, the model is most applicable for low-Weber-number collisions where collisions result in bouncing and coalescence. FLUENT offers two spray breakup models: the Taylor Analogy Breakup (TAB) model and wave-model. In the present study, the TAB model was used to simulate the droplet breakup. This model is applicable for Weber number less than 100. Accurate determination of droplet drag coefficient is crucial for accurate spray modelling. In this project work, a dynamic drag model was used to account for variations of the droplet shape. More details of droplet collision model, TAB model and dynamic drag model can be found in the FLUENT™ User Guide.

3.2.2 Heat and mass transfer models

Three models corresponding to following three different regimes of heat and mass transfer between the dispersed and continuous phases were considered.

- Inert heating
- Vaporization
- Boiling

Inert heating

For the liquid droplet when its temperature is less than the vaporization temperature T_{vap} of the droplet and/or when all the volatile mass of the drop is evaporated, the inert heating was considered. These conditions may be written as (Sommerfeld, 1993):

$$\begin{aligned} T_D &\le T_{vap} \\ m_D &\le (1 - f_{v0}) m_{D0} \end{aligned} \tag{5}$$

Where T_D is droplet temperature, T_{vap} is the vaporization temperature, m_{D0} is the initial mass of the droplet, m_D is the current mass of drop and f_{v0} is mass fraction of the volatile components. When these conditions are satisfied, the following heat balance equation was used to relate the drop temperature $T_D(t)$ to the convective heat transfer:

$$m_D C p_D \frac{dT_D}{dt} = h A_D \left(T_\infty - T_D \right) \tag{6}$$

Where h is the heat transfer coefficient calculated using Ranz and Marshall (Gouesbet and Berlemont, 1999; Sommerfeld, 1990) and T_∞ is the continuous phase temperature.

Vaporization from drop

When the evaporation of liquid phase starts, it is essential to consider the mass transfer as well as heat transfer from the drop surface. This regime of droplet heating was initiated when the temperature of the droplet reaches the vaporization temperature, T_{vap} and continues until droplet reaches the boiling point, T_{bp}, or until the droplet's volatile fraction is completely consumed (Sommerfeld, 1990):

$$\begin{aligned} T_D &< T_{bp} \\ m_D &> (1 - f_{v0}) m_{D0} \end{aligned} \tag{7}$$

Mass transfer: The rate of vaporization was modelled by relating the flux of droplet vapor into the gas phase to the gradient of the vapor concentration between the droplet surface and the bulk gas as (Gouesbet and Berlemont, 1999):

$$N_i = k_c a\left(C_{i.s} - C_{i,\infty}\right) \tag{8}$$

The concentration of vapor at the droplet surface is evaluated by assuming that the partial pressure of vapor at the interface is equal to the saturated vapor pressure, P_{sat}, at the particle droplet temperature, T_D:

$$C_{i,s} = \frac{P_{sat,T_D}}{RT_D} \tag{9}$$

where R is the universal gas constant.

$$C_{i,\infty} = X_i \frac{P_{op}}{RT_\infty} \tag{10}$$

where Xi is local bulk mole fraction of species i, P_{op} is the operating pressure and T_∞ is the local bulk temperature in the gas. The mass transfer coefficient k_c was calculated using the correlation of Sherwood and Pigford (Sommerfeld, 1993):

$$Sh = 2 + 0.5252 * \text{Re}^{0.5}\, Sc^{0.33} \tag{11}$$

The mass of droplet reduced to

$$m_D\left(t + \Delta t\right) = m_D\left(t\right) - N_i A_D M_i \Delta t \tag{12}$$

Where M_i is the molecular weight of species i and m_D is the mass of the droplet.
Heat transfer: The droplet temperature was updated according to a heat balance that relates the sensible heat change in the droplet to the convective and latent heat transfer between the droplet and the gas:

$$m_D Cp_D \frac{dT_D}{dt} = hA\left(T_D - T_\infty\right) + \frac{dm_D}{dt}\lambda \tag{13}$$

Boiling from the drop

This phase was initiated when the temperature of the droplet has reached the boiling temperature, T_{bp}, and while the mass of the droplet exceeds the non-volatile fraction, $(1 - f_{v0})$:

$$\begin{aligned} T_D &\geq T_{bp} \\ m_D &\geq \left(1 - f_{v0}\right) m_{D0} \end{aligned} \tag{14}$$

When the droplet temperature reaches the boiling point, a boiling rate equation is applied (Sommerfeld, 1993)

$$\frac{d\left(d_D\right)}{dt} = \frac{4k_\infty}{\rho_D Cp_\infty d_D}\left(1 + 0.23\sqrt{\text{Re}_d}\right)\ \ln\left[1 + \frac{Cp_\infty\left(T_\infty - T_D\right)}{hf_g}\right] \tag{15}$$

Where, Cp_∞ is the specific heat of gas (J/kg-K), ρ_D is the density of drop (kg/m^3) and k_∞ is the thermal conductivity of the gas (W/m-K). Note that the model requires $T_\infty > T_{bp}$ in order for boiling to occur and that the droplet remains at fixed temperature (T_{bp}) throughout the boiling law.

Mass transfer of gas phase component to drop

The rate of C_2 mass transfer was modelled by relating the flux of C_2 into the droplet to the differential of the C_2 concentration between the bulk gas and droplet surface as

$$N_i = k_g a\left(C_{i,\infty} - C_{i,s}\right) \tag{16}$$

The concentration of vapor at the droplet surface is evaluated by assuming that the partial pressure of vapor at the interface is equal to the saturated vapor pressure, P_{sat} , at the particle droplet temperature, T_D:

$$C_{i,s} = \frac{P_{sat,T_D}}{RT_D} \tag{17}$$

where R is the universal gas constant.

$$C_{i,\infty} = y_i \frac{P_{op}}{RT_\infty} \tag{18}$$

where y_i is local bulk mole fraction of species i, P_{op} is the operating pressure and T_∞ is the local bulk temperature in the gas. The mass transfer coefficient k_g was calculated using Equation 8.

3.2.3 Polymerization reaction

Some polymerizations can be characterized by chain initiation, chain propagation, chain transfer, chain termination, and catalyst deactivation. Obtaining their *absolute* rates as a function of process conditions is the ultimate goal of the kinetic studies. However, in some solution polymerization processes, the majority of the kinetic studies are on the *relative* polymerization kinetic rates, which enables modelling of polymer properties as well as quantification of the overall material balance for the reactors. Different and more accurate experimental methods are required to estimate the absolute kinetics than are used to develop the relative ones. In many instances, the absolute chain propagation and the catalyst deactivation rate constants are used for the catalyst efficiency. The reaction rate is obtained by multiplying the catalyst flow rate by catalyst efficiency. The catalyst efficiency expression used in the present work is:

$$E = K^* \frac{k_p}{k_d}[C_{monomer}]\theta \tag{19}$$

where, E is the catalyst efficiency [lb polymer/lb catalyst], K^* is an empirical constant, θ is the reactor residence time [s], k_p is the propagation rate constant [1/s/(mol/L)], and k_d is the catalyst deactivation rate constant [1/s].

3.2.4 Influence of shroud velocity

Shape and extent of the dilute zone formed by a jet in a reactor is controlled by different process parameter such as support tube exit velocities and nozzle design [11]. The shape of dilute zone and local fluid dynamics in the dilute zone determines the dispersion of the liquid catalyst in the dilute zone. Simulations were therefore carried out for two different support tube exit velocities, viz. 16 m/s and 32 m/s. The predicted velocity contours at the vertical plane cutting through the nozzle are shown in Figure 18. It can be seen from Figure 18 that the jet coming out of the nozzle first travels horizontally and then turns to the upward direction. Momentum balance between the nozzle jet and bottom feed determines the shape and extent of jet and therefore the dilute zone in the reactor. The model predictions show better shroud flow at a higher support tube exit velocity.

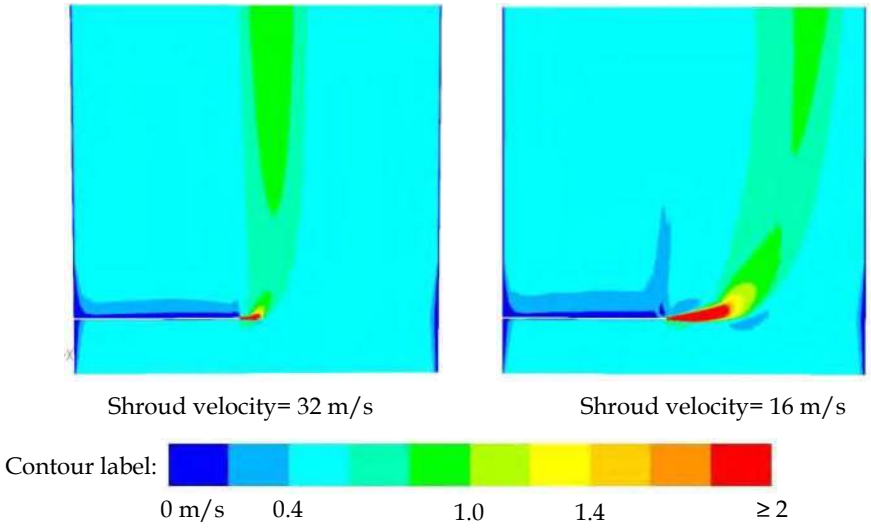

Fig. 18. Predicted Velocity Magnitude Distribution at *r-z* Plane Cutting through Nozzle for Different Shroud Flow Rates

The CFD model was then extended to simulate the dispersion of catalyst droplets. DPM simulations were carried out to simulate the trajectories of the catalyst droplets without evaporation of solvent. Catalyst droplets were injected into reactor from the catalyst inlet of the nozzle. Inlet boundary conditions such as the drop size distribution, mass flow rate and velocity of the drops are very important. In the present work, experimentally measured drop size distribution fitted using the Rosin Rammler distribution was specified at inlet. The distribution parameters are thus: minimum diameter equal to 15 microns, maximum diameter equal to65 microns, mean diameter equal to 31.25 microns, and width of distribution equals to 1.6. Drops were injected into the reactor with a velocity equal to the atomizing gas velocity and a velocity of 150 m/s. The predicted snapshots of droplet dispersion for both tube velocities are shown in Figure 19.

A few conclusions can be drawn from the predicted snapshots shown in Figure 19. The shape of dilute zone determines the trajectories of the droplets. For the 16 m/s tube velocity, the injected drops first move in the horizontal direction and are accumulated at the end of the dilute zone before moving up. Strong deceleration of the droplets along the jet and

sudden upward movement of jet might be responsible for this kind of dispersion. Such dispersion may cause strong interactions between droplets and lead to coalescence of the droplets or agglomeration of particles. On the other hand, the quality of dispersion is significantly improved when the support tube velocity is increased to 32 m/s. The increase in the tube velocity not only improves the shroud flow, but also significantly minimizes the extent of accumulation of droplets in the dilute zone. The predicted drop size distributions were converted into volumetric distributions. Such information is helpful for comparisons with the inlet distribution and gives insights into the chemical reaction in the dilute zone. The comparison of the predicted droplet size distributions at two different flow times (20 milliseconds and 40 milliseconds respectively) for both support tube exit velocities is shown in Figure 20 together with the inlet distribution. It can be seen from Figure 20 that compared to the higher support tube flow, the predicted diameter distribution significantly moves toward the right direction for the lower support tube flow. It was also observed that the predicted distribution further moves to the right as the droplets proceeds with the flow. This suggests more coalescence in the dilute zone for the 16 m/s support tube velocity. Figure 20 also shows very promising results with the support tube velocity equal to 32 m/s. The predicted droplet size distribution after 20 milliseconds for the 32 m/s feed velocity is very close to the inlet size distribution. Similar to 16 m/s results, the predicted drop distribution moves to the right with an increase in flow time. The results show much smaller volume fraction of larger droplets with the feed rate of 32 m/s than 16 m/s.

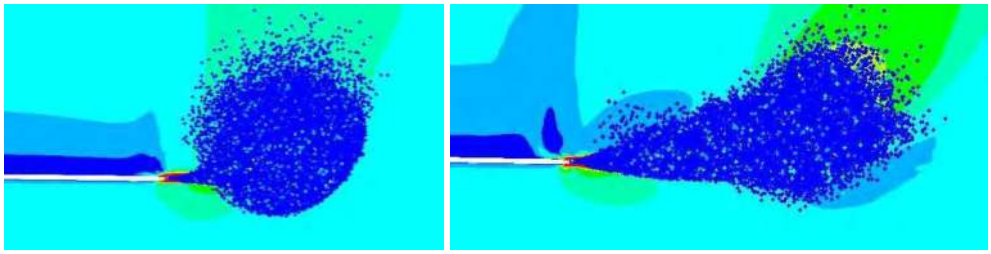

(a) Shroud velocity= 16 m/s (b) Shroud velocity= 32 m/s

Fig. 19. Predicted Snapshots of Droplet Dispersion in Dilute Zone at Three Different Time Intervals

A polymerization reaction in a drop is a bulk or volumetric reaction. Therefore, the rate of polymer formation is directly dependant on the volume of the drop. It is possible to have different polymer formation rate for different droplet sizes. A separate model was developed to simulate the mass transfer of monomer from gas phase to droplet and simultaneous polymerization reaction. This model was then incorporated into the CFD model using user defined functions (UDF's). The predicted results were used to shed some light on the particle growth process. The particle growth rate was estimated using predicted particle size. The predicted values of particle growth rate at different time intervals are shown in Figure 21. Few conclusions can be drawn from Figure 21. First, for both the particles, the rate of particle growth is very fast at the beginning. The particle growth rate then slows down. Second, the particle growth rate is comparatively very fast for bigger droplets than smaller droplets. This indicates that the larger droplets grow much faster than the smaller droplets and can form bigger particles. This phenomenon will influence the individual particle growth when different size droplets are fed into the reactor. Different particle growth rates also highlight the possibility of having different rate controlling steps

for polymerization reaction. The predicted growth rate suggests the possibility of having kinetically controlled reaction in the smaller drops due to smaller drop volume. Whereas, it is possible that reaction kinetics may not control the growth of bigger droplets.

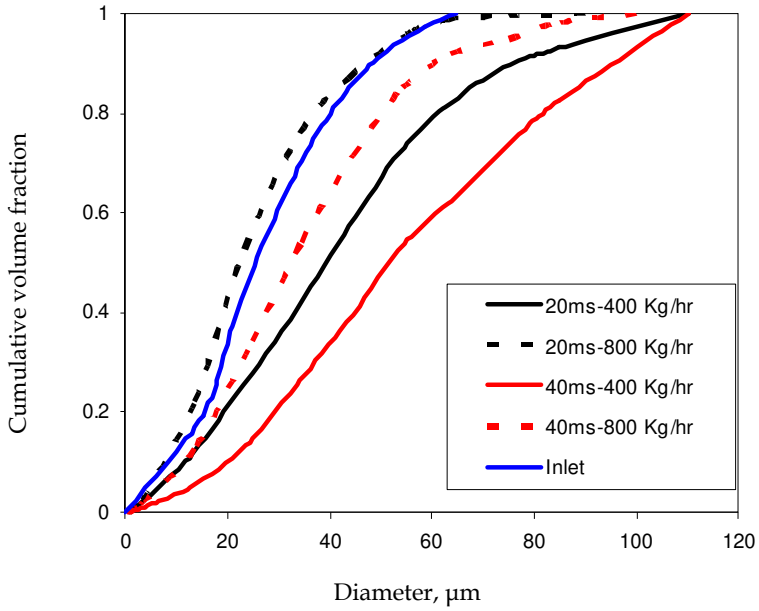

Fig. 20. Influence of Support Tube Exit Velocity on Drop Diameter Distribution at 20 Milliseconds and 40 Milliseconds

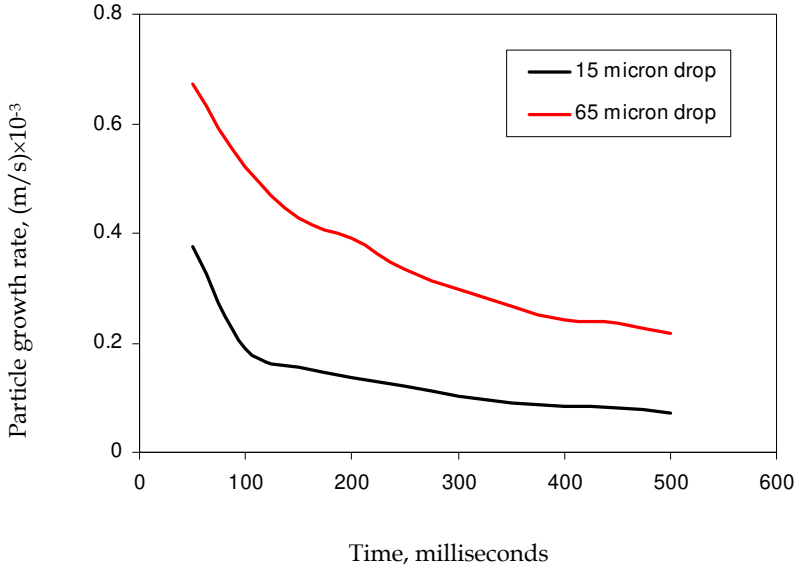

Fig. 21. Predicted Influence of Drop Size on Particle Growth Rate

It is of the interest to understand the influence of support tube velocity on the particle growth process due to polymerization reaction. The predicted particle size distributions at different time intervals for both the shroud velocity were then compared. The comparison of predicted particle size distribution for both the support tube flow rates is shown in Figure 22. It can be seen from Figure 22 that the higher support tube flow rate significantly influenced the particle

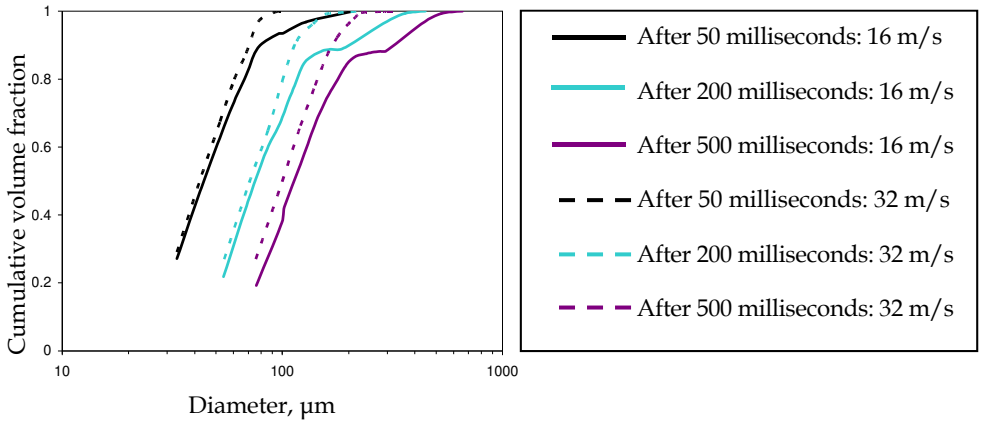

Fig. 22. Influence of Support Tube Flow Rate on Predicted Particle Diameter Distribution

size distribution in reactor. It was observed that the better shroud flow not only controlled the rapid growth of the bigger particles but also significantly minimized the total volume fraction of the bigger drops present in the distribution. The obtained narrow particle size distribution at higher support tube flow rate suggests the possibility of having kinetic controlled polymerization reaction in almost all the fed droplets. Lower coalescence rate and reaction into kinetically controlled regime with higher shroud velocity will help to control the particle size distribution in the reactor.

3.3 Summary of numerical modeling

In this chapter, we have demonstrated the application of computational fluid dynamics (CFD) models for simulating reactive sprays. The present work highlighted the applicability of CFD models based on the Eulerian-Eulerian and Eulerian-Lagrangian approaches for simulating reactive sprays. Despite some of the limitations, computational models were shown to provide useful information on the transport processes occurring in the dilute zone. The computational models were able to predict the implications of operating conditions and dispersion of droplets in the dilute zone on the transport process and subsequent particle growth. Careful numerical experiments using these CFD models can be used for better understanding the characteristics of existing spraying operation, to enhance its performance, assess different configurations and greatly assist the engineering decision making process. The approaches, sub-models and the results discussed here will provide a useful basis for practical applications as well as for further developments.

Although the models discussed here are capable of providing valuable and new insights which hitherto were unavailable, there is still significant scope to improve the fidelity of these models.

- Important and intellectually challenging fluid dynamic and transport phenomena occur at different length and time scales with sprays. On the micron scale, boundary layers and wake develop because of relative motion between drops and the gas. In addition to this, there are abundant complicated fluid dynamics factor at this length scale: shear driven internal circulation of the liquid in the droplet, Stefan flow due to vaporization and condensation, hydrodynamic interfacial instabilities leading to droplet shape distortion and subsequent droplet shattering and droplet interaction with the free stream turbulence of gas phase. Whereas, on the coarser scale, we have complexities associated with the exchanges of mass, momentum and energy of many droplets in the some sub-volume of interest and process by which a coherent liquid flow disintegrates into droplets. The problem becomes very complicated because of the strong coupling possesses by these different scales. One cannot explain the processes on the coarser scale without detail knowledge of the fine-scale phenomena. Note that in some practical problems, the disparity of length scale differ by several orders of magnitude so that a challenging subgrid modeling problem results. Actually, direct numerical simulation (DNS), where all the flow scales are resolved, could provide valuable insight. However, carrying out DNS of a complete spraying operation is a huge challenge due to computational cost. Large eddy simulation (LES), where only large scale turbulence is resolved can improve the accuracy of the spray simulation compared to the Reynolds averaged approaches (RANs). However, the required models for simulating multi-physics of spraying operations are often non-existent or lack the desired accuracy.
- Characterization of primary atomization represents a challenge for experiments. Numerical modeling should provide a much needed alternative. However, numerical studies of primary atomization are also sparse. No clear gold standard has emerged on how to conduct a numerical simulation of complex two-phase flows. Therefore, several key issues such as the discontinuous nature of the flow properties across the phase-interface, the singularity of the surface tension forces, and the very large range of scales involved in atomization remain unanswered.

Adequate attention to key issues mentioned above and the creative use of computational flow modeling will hopefully make useful contributions to industrial spraying operation.

4. Acknowledgements

The following individuals are gratefully acknowledged for their help in acquiring the various images presented throughout this chapter: Kuide Qin, Charles Lipp, Pramod Patil, Billy Smith, Santhosh Ramalingam, Mike Trippeer, and Rugved Pathare.

5. References

Bini, M., Jones, W.P. and Lettieri, C. 2009, Large Eddy Simulation of spray atomization with stochastic modelling of breakup, *Proceedings of the European Combustion Meeting*.

Brackbill, U., Kothe, D.B., Zemch, C.: "A Continuum Method for Modeling Surface Tension", Journal of Computational Physics, 1992(100), pp.335-354.

Gorokhovski, M. and Herrmann, M. 2008, Modeling primary atomization, *Annual Rev. Fluid Mech.*, 40, 343-366.

Gouesbet, G. and Berlemont, A., Eulerian and Lagrangian approaches for predicting the behavior of discrete particles in turbulent flows, *Prog. Energy Combustion Sci.* (1999), 25, pp. 133–159.

Hirt, C.W., Nichols, B.D.: "Volume of Fluid (VOF) Method for The Dynamics of Free Boundaries", Journal of Computational Physics, 1981(39), pp.201-225.

Liu, W., Garrick, S., and Cloeter, M.D., *Large-scale Simulation of Sprays with Adjuvants and Non-Newtonian Fluids*, Poster ILASS2011-P06, ILASS-Americas 23rd Annual Conference on Liquid Atomization and Spray Systems, Ventura, CA, May 2011.

Muzaferija, S., Peric, M., Sames, P. and Schellin, T.: "A Two-Fluid Navier-Stokes Solver to Simulate Water Entry", in Proc. 22nd Symposium on Naval Hydrodynamics, Washington D.C., 1998, pp.277-289.

Osher, S., Sethian, J.A.: "Fronts Propagating with Curvature-Dependent Speed: Algorithms Based on Hamilton-Jacobi Formulations", Journal of Computational Physics 1988(79), pp.12-49.

O'Rourke, P.J., *Collective Drop Effects on Vaporizing Liquid Sprays,* PhD thesis, Princeton University, Princeton, New Jersey, 1981.

Patterson, M.A., Reitz, R.D.: "Modeling the Effects of Fuel Characteristics on Diesel Engine Combustion and Emission", SAE 980131, 1998.

Raffel, M., Willert, C.E., and Kompenhans, J., *Particle Image Velocimetry. A Practical Guide*, Springer-Verlag, Berlin, 1998.

Ranade, V.V., *Computational Flow Modelling for Chemical Reactor Engineering*, Academic Press, New York, 2002.

Reitz, R.D., Diwakar, R.: "Structure of High Pressure Fuel Spray", SAE Technical Paper Series 870598, 1987.

Sommerfeld, M., Reviews in numerical modeling of dispersed two phase flows, *Proceedings of 5th Int. Symp. on Refined Flow Modeling and Turbulence Measurements*, Paris, 1993.

Sommerfeld, M., Numerical simulation of the particle dispersion in turbulent flow: the importance of particle lift forces and particle/wall collision models, in *Numerical Methods for Multiphase Flows*, Vol. 91, ASME, New York, 1990.

Sussman, M., Smereka, P. and Osher, S.: "A Level Set Method for Computing Solutions to Incompressible Two-Phase Flow", Journal of Computational Physics, 1994(114), pp.146-159.

Thomson, D.J., Criteria for the selection of stochastic models of particle trajectories in turbulent flows, *J. Fluid Mech.* (1987), 180, pp. 529–556.

Ubbink, O.: "Numerical Prediction of Two Fluid Systems with Sharp Interface", Ph.D. thesis, Imperial College of Science, Technology and Medicine, London, England, 1997.

Unverdi, S.O., Tryggvason, G.: "A Front Tracking Method for Viscous, Incompressible, multi-fluid flows", Journal of Computational Physics, 1992 (100), pp.25-37.

Youngs, D.L.: "Time-Dependent Multi-Material Flow with Large Fluid Distortion", Numerical Methods for Fluid Dynamics, Academic Press, 1982.

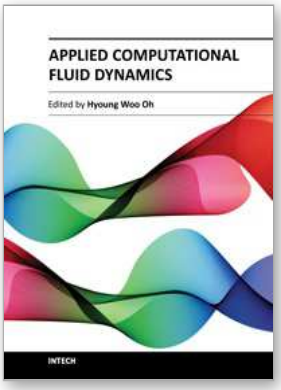

Applied Computational Fluid Dynamics

Edited by Prof. Hyoung Woo Oh

ISBN 978-953-51-0271-7
Hard cover, 344 pages
Publisher InTech
Published online 14, March, 2012
Published in print edition March, 2012

This book is served as a reference text to meet the needs of advanced scientists and research engineers who seek for their own computational fluid dynamics (CFD) skills to solve a variety of fluid flow problems. Key Features: - Flow Modeling in Sedimentation Tank, - Greenhouse Environment, - Hypersonic Aerodynamics, - Cooling Systems Design, - Photochemical Reaction Engineering, - Atmospheric Reentry Problem, - Fluid-Structure Interaction (FSI), - Atomization, - Hydraulic Component Design, - Air Conditioning System, - Industrial Applications of CFD

INTECH
open science | open minds

InTech Europe
University Campus STeP Ri
Slavka Krautzeka 83/A
51000 Rijeka, Croatia
Phone: +385 (51) 770 447
Fax: +385 (51) 686 166
www.intechopen.com

InTech China
Unit 405, Office Block, Hotel Equatorial Shanghai
No.65, Yan An Road (West), Shanghai, 200040, China
中国上海市延安西路65号上海国际贵都大饭店办公楼405单元
Phone: +86-21-62489820
Fax: +86-21-62489821